

Magnetic phase diagram of CuO

R. Villarreal,^{1,*} G. Quirion,¹ M.L. Plumer,¹ M. Poirier,² T. Usui,³ and T. Kimura³

¹*Department of Physics and Physical Oceanography,*

Memorial University, St. John's, Newfoundland, Canada, A1B 3X7

²*Département de Physique, Université de Sherbrooke, Sherbrooke, Québec J1K 2R1, Canada*

³*Division of Materials Physics, Osaka University, Toyonaka, Osaka, Japan*

(Dated: June 22, 2018)

High resolution ultrasonic velocity measurements have been used to determine the temperature – magnetic-field phase diagram of the monoclinic multiferroic CuO. A new transition at $T_{N3} = 230$ K, corresponding to an intermediate state between the antiferromagnetic non-collinear spiral phase observed below $T_{N2} = 229.3$ K and the paramagnetic phase, is revealed. Anomalies associated with a first order transition to the commensurate collinear phase are also observed at $T_{N1} = 213$ K. For fields with $\mathbf{B} \parallel \mathbf{b}$, a spin-flop transition is detected between 11 T - 13 T at lower temperatures. Moreover, our analysis using a Landau-type free energy clearly reveals the necessity for an incommensurate collinear phase between the spiral and the paramagnetic phase. This model is also relevant to the phase diagrams of other monoclinic multiferroic systems.

PACS numbers: 75.10.-b, 75.30.Kz, 75.85.+t, 75.30.Gw

Multiferroic phenomena have been a subject of intense interest in recent decades arising from opportunities to explore new fundamental physics as well as possible technological applications [1–3]. Coupling between different ferroic orders has been proven to be driven by several different types of mechanisms. In particular, multiferroics with a spiral spin-order-induced ferroelectricity have revealed high spontaneous polarization and strong magnetoelectric coupling [4, 5]. Cupric oxide (CuO), the subject of this letter, was characterized as a magnetoelectric multiferroic four years ago when it was shown that its ferroelectric order is induced by the onset of a spiral antiferromagnetic (AFM) order at an unusually high temperature of 230 K [3]. Thus far, two AFM states have been reported, a low temperature ($T_{N1} \sim 213$ K) AF1 commensurate collinear state with the magnetic moments along the monoclinic \mathbf{b} axis and an AF2 incommensurate spiral state with half of the magnetic moments in the ac plane ($T_{N2} \sim 230$ K) [3, 6, 7]. However, the authors of the neutron diffraction measurements [6] questioned the possibility of having a direct condensation from a paramagnetic (PM) phase to a spiral magnetic phase. Despite this remark, a recent Landau theory [8], as well as several Monte-Carlo simulations [9, 10], appear to support this sequence of magnetic orderings.

Encouraged by recent experiments on other multiferroic systems using ultrasonic measurements [11], we measured the temperature and field dependence of the velocity of transverse modes in order to determine the magnetic phase diagram of CuO. A new transition is detected at $T_{N3} = 230$ K just above the AF2 spiral phase observed at $T_{N2} = 229.3$ K, while the first order transition is observed at $T_{N1} = 213$ K. Furthermore, dielectric constant measurements confirm that only the spiral phase (between T_{N1} and T_{N2}) supports a spontaneous electric polarization. In addition, we report on a spin-flop tran-

sition in the low temperature AF1 collinear phase when $\mathbf{B} \parallel \mathbf{b}$. Thus, based on these findings, a new magnetic-field *vs* temperature phase diagram is proposed for CuO.

In order to elucidate the possible nature of the AFM states observed in CuO, a non-local Landau-type free energy is also developed for CuO and similar monoclinic multiferroics. This approach has been very successful in explaining the magnetic phase diagrams of other multiferroic systems [12–14]. In contrast with the conclusions of Refs. [8–10], our analysis based on rigorous symmetry arguments indicates that there must be a collinear intermediate phase (AF3) between the paramagnetic and spiral AF2 states. Such a phase has been shown, both theoretically and experimentally, to occur in other geometrically frustrated antiferromagnets where symmetry allows for uniaxial anisotropy at second order [14, 15]. Finally, we compare the model predictions to the B-T phase diagram of CuO obtained using ultrasonic velocity data. Similarities with other multiferroic systems such as MnWO_4 , AMSi_2O_6 , RMnO_3 , RMn_2O_5 , and $\text{Ni}_3\text{V}_2\text{O}_8$ are also noted.

For the purpose of this study, a CuO sample was grown using a floating zone technique as described in Ref. [3]. A single crystal was cut with faces perpendicular to the monoclinic axes \mathbf{a}^* , $\mathbf{b}^* = \mathbf{b}$, and \mathbf{c}^* ($4 \times 4 \times 3$ mm³). The sample was then polished to obtain parallel faces. For velocity measurements, plane acoustic waves were generated using 30 MHz LiNbO_3 piezoelectric transducers bonded to opposite faces. Using an ultrasonic interferometer, which measures the phase shift and the amplitude of the first elastic transmitted pulse, high-resolution relative velocity variations ($\Delta V/V \sim 1$ ppm) were achieved. Experimental data presented here were all obtained using the velocity of transverse waves $V_{a^*}[c^*]$ propagating along the \mathbf{a}^* axis and polarized along \mathbf{c}^* , with the magnetic field applied along the easy magnetic axis of CuO

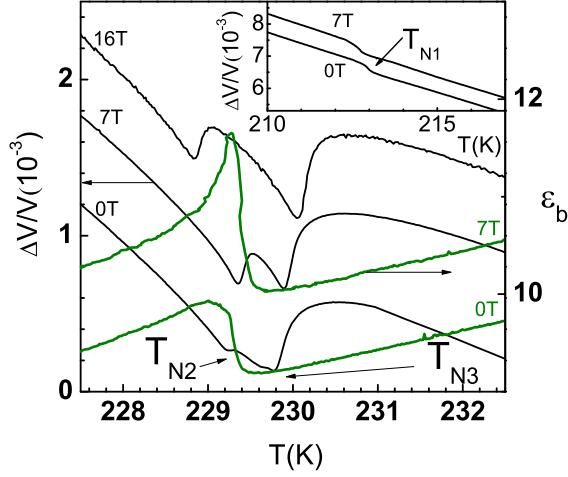


FIG. 1. Temperature dependence of the dielectric constant ϵ_b (in green) and the relative velocity variations of transverse mode $V_{a^*}[c^*]$ measured at different fields with $\mathbf{B} \parallel \mathbf{b}$.

(\mathbf{b} axis). Simultaneous capacitance measurements were carried out using an AH 2550A Ultra Precision 1kHz Capacitance Bridge to identify which of these phases are ferroelectric. For that purpose, electrodes were mounted on faces perpendicular to the \mathbf{b} axis in order to determine the dielectric constant ϵ_b .

Fig. 1 shows the temperature dependence of the relative sound velocity variations ($\Delta V/V$) for $\mathbf{B} \parallel \mathbf{b}$. At zero field, the anomaly observed at $T_{N1} = 213$ K (see inset of Fig. 1) coincides very well with the onset of a commensurate collinear antiferromagnetic state. Our high resolution velocity measurements also reveal *two* anomalies at $T_{N2} = 229.3$ K and $T_{N3} = 230.0$ K near the stabiliza-

tion of a spiral order previously determined by neutron diffraction and susceptibility measurements [3, 6], which were thought to occur at a single transition. At higher fields, the amplitude of the step like variation observed at 229.3 K, as well as the temperature difference between T_{N2} and T_{N3} increases, confirming the existence of a new intermediate magnetic order AF3. This finding is supported by dielectric measurements also shown in Fig. 1. Notice that, as the stability range of the intermediate phase is small ($\Delta T \sim 0.7$ K), velocity and dielectric data have been collected simultaneously to avoid any ambiguity regarding the actual critical temperatures. Thus, as shown in Fig. 1 (for $B = 0$ and 7 T), the anomaly observed on the dielectric constant ϵ_b coincides very well with T_{N2} determined using velocity data, while no variation is noticeable at T_{N3} . These results also indicate that the new phase AF3 is not ferroelectric, while magneto-electric coupling exists for the AF2 phase.

We present in Fig. 2 the magnetic phase diagram of CuO determined up to 16 T using ultrasonic velocity measurements for $\mathbf{B} \parallel \mathbf{b}$. The inset of Fig. 2 shows the field dependence of the velocity which displays a minimum around 11 T for $T = 125$ K. As the magnetic moments are known to be parallel to the field in the AF1 commensurate collinear state [3, 6], we attribute this anomaly to a spin-flop transition [16]. In summary, while the critical temperatures T_{N1} , T_{N2} , and T_{N3} are weakly field dependent, the spin-flop critical field H_{SF} increases with temperature. At 10 K, $H_{SF} = 11$ T and increases slowly up to 13.5 T at T_{N1} , in good agreement with magnetic susceptibility measurements performed on powder samples [17].

Since no neutron scattering data exists for the HF1 and AF3 states, we develop a Landau-type model in order to elucidate the nature of these new magnetic orders [14, 15]. The integral form of the free energy is expanded in powers of the nonlocal spin density $\mathbf{s}(\mathbf{r})$ defined in terms of a uniform field-induced magnetization \mathbf{m} and a spin polarization vector \mathbf{S} modulated by a single wave vector \mathbf{Q} describing the long-range magnetic order (Eq. (6) of Ref. [14]). Within the present model, the value of \mathbf{Q} can be determined by simply considering the isotropic quadratic contribution

$$F_{2I} = \frac{1}{2V^2} \int d\mathbf{r}_1 d\mathbf{r}_2 A(\mathbf{r}_1 - \mathbf{r}_2) \mathbf{s}(\mathbf{r}_1) \cdot \mathbf{s}(\mathbf{r}_2), \quad (1)$$

which leads to $F_{2I} = \frac{1}{2} \tilde{A} m^2 + A_Q S^2$ where $A_Q = aT + J_Q$, with J_Q being the Fourier transform of the exchange integral $J(\mathbf{R})$. Considering the C-type monoclinic cell with four Cu^{2+} magnetic ions, we obtain

$$\begin{aligned} J(\mathbf{Q}) &= 2[J_1 f_1(\mathbf{Q}) + J_2 f_2(\mathbf{Q}) + J_3 f_3(\mathbf{Q}) + J_4 f_4(\mathbf{Q})] \\ f_1(\mathbf{Q}) &= \cos(\pi q_a - \pi q_c) \\ f_2(\mathbf{Q}) &= \cos(\pi q_a + \pi q_c) \\ f_3(\mathbf{Q}) &= \cos(\pi q_a - \pi q_b) + \cos(\pi q_a + \pi q_b) \\ f_4(\mathbf{Q}) &= \cos(\pi q_b - \pi q_c) + \cos(\pi q_b + \pi q_c), \end{aligned} \quad (2)$$

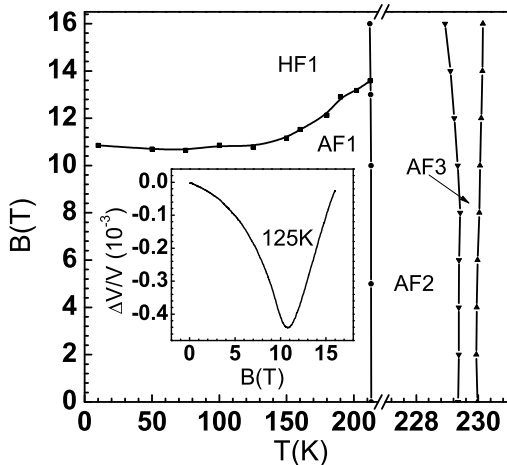


FIG. 2. Magnetic phase diagram of CuO for $\mathbf{B} \parallel \mathbf{b}$. Inset shows the relative velocity variation of $V_{a^*}[c^*]$ as a function of the field for $T = 125$ K.

where J_1 and J_2 represent the nearest-neighbors (NN) exchange interactions along the AFM-chain (sites 2-3) and the coupling between chains (sites 1-4) on the same plane normal to \mathbf{b} , respectively, and J_3 and J_4 represent the exchange interactions along \mathbf{a} (sites 1-2) and \mathbf{c} (sites 1-3) between ions on different planes (see Fig. 4). The value of \mathbf{Q} is then obtained by finding the extrema of J_Q (Eq. 2) as a function of the exchange interactions. Results of our numerical algorithm are summarized in the J_2 – J_3 phase diagram shown in Fig. 3 for AFM chains ($J_1 = 1$). For different J_4 values, we obtain three phases: an incommensurate phase with $\mathbf{Q}_{ICM} = [q_a, 0, q_c]$ (left side) and two commensurate phases (top and bottom right side). Depending on the sign of J_3 relative to J_4 , the commensurate wave vector is either $\mathbf{Q}_{CM} = [100]$ or $\mathbf{Q}_{CM} = [001]$. More interestingly, with $J_3 = J_4 = 0$ we obtain the expected commensurate wave vector $\mathbf{Q}_{CM} = [\frac{1}{2} \ 0 \ -\frac{1}{2}]$ for $J_2 \leq 0$ (dash line in Fig. 3). Moreover, an ICM state with a modulation vector comparable to that of the experimental value $\mathbf{Q}_{ICM} = [0.506 \ 0 \ -0.483]$ is stabilized whenever J_3 and/or J_4 are non-zero but small relative to J_1 (for example, $J_2/J_1 = -0.3$, $J_3/J_1 = 0.017$, and $J_4/J_1 = 0$ leading to $J_Q/J_1 = -2.6$). These relative values are also in good agreement with estimates obtained by density functional theory [9, 18, 19] and are consistent with the quasi-1D magnetic character of CuO.

In addition to the usual isotropic second order exchange term, we also consider anisotropic contributions. Considering the symmetry of monoclinic crystals ($C2/c$), we identified three invariants, written in single-ion form as

$$F_{2A} = \frac{1}{2V} \int [D_y(\mathbf{r})s_y(\mathbf{r})s_y(\mathbf{r}) + D_z(\mathbf{r})s_z(\mathbf{r})s_z(\mathbf{r})$$

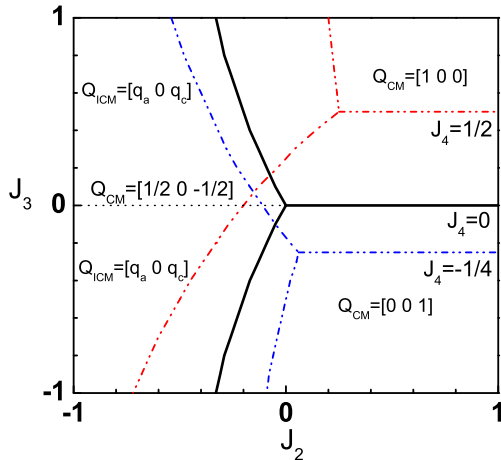


FIG. 3. J_3 – J_2 phase diagram for different values of J_4 with $J_1 = 1$. One incommensurate phase with $\mathbf{Q}_{ICM} = [q_a, 0, q_c]$ (left side) and two commensurate phases ($\mathbf{Q}_{CM} = [100]$ and $\mathbf{Q}_{CM} = [001]$) are obtained.

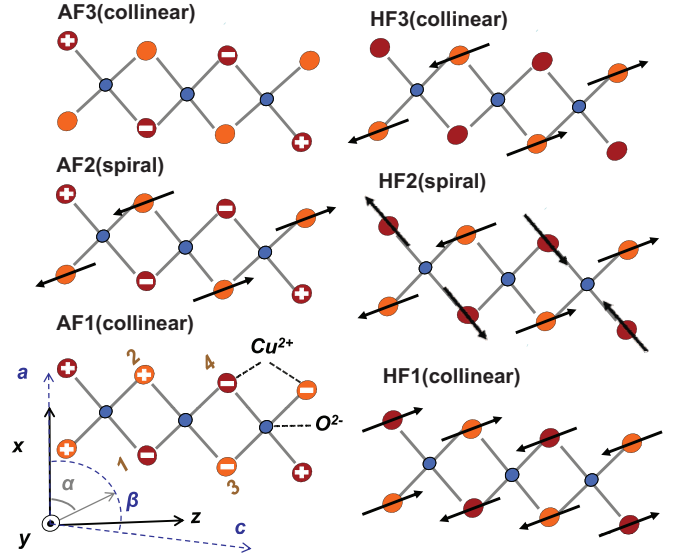


FIG. 4. Spin configurations in a magnetic cell of 8 ions (red and orange circles). Red circles represent magnetic ions at $b = 1/2$. The \pm symbols represent spins in/out of the page. When no direction is specified (as in AF3 and HF3), spins on these sites are not ordered.

$$+ D_{xz}(\mathbf{r})s_x(\mathbf{r})s_z(\mathbf{r})] d\mathbf{r} . \quad (3)$$

While D_y can be used to set the magnetic easy axis along \mathbf{b} , the other terms are necessary in order to define the direction of the moments in the ac plane. Furthermore, to account for non-collinear spin configurations, we define $\mathbf{S} = \mathbf{S}_1 + i \mathbf{S}_2$, with

$$\begin{aligned} \mathbf{S}_1 &= S \cos \beta [\cos \gamma \hat{\mathbf{y}} + \sin \gamma \hat{\rho}_2], \\ \mathbf{S}_2 &= S \sin \beta [\cos \theta \hat{\rho}_1 + \sin \theta (\cos \gamma \hat{\mathbf{y}} + \sin \gamma \hat{\rho}_2)], \end{aligned} \quad (4)$$

where $\hat{\rho}_1$ and $\hat{\rho}_2$ are two orthogonal unit vectors normal to the easy axis, $\hat{\mathbf{y}} \parallel \mathbf{b}$. Thus, the direction of the moments in the ac plane is accounted for by defining the unit vectors $\hat{\rho}_1$ and $\hat{\rho}_2$ relative to the lattice vectors, $\hat{\rho}_1 = \cos \alpha \hat{\mathbf{x}} + \sin \alpha \hat{\mathbf{z}}$ and $\hat{\rho}_2 = -\sin \alpha \hat{\mathbf{x}} + \cos \alpha \hat{\mathbf{z}}$. As shown in Fig. 4, the parameter α represents the angle between the ac plane component of \mathbf{S} relative to the monoclinic axis $\mathbf{a} \parallel \hat{\mathbf{x}}$. After integration, all second-order contributions for $\mathbf{m} \parallel \mathbf{H} \parallel \hat{\mathbf{y}}$ reduce to

$$\begin{aligned} F_2^{total} &= \frac{1}{2} \tilde{A}_0 m^2 + A_Q S^2 - \frac{1}{2} D_{y0} m^2 - D_{yQ} |S_y|^2 \\ &\quad - D_{zQ} |S_z|^2 + D_{xzQ} S_x S_z - \mathbf{H} \cdot \mathbf{m}. \end{aligned} \quad (5)$$

Adopting the same approach for the fourth-order isotropic term, we obtain

$$\begin{aligned} F_{4I} &= B_1 S^4 + \frac{1}{2} B_2 |\mathbf{S} \cdot \mathbf{S}|^2 + \frac{1}{4} B_3 m^4 + 2 B_4 |\mathbf{m} \cdot \mathbf{S}|^2 \\ &\quad + B_5 m^2 S^2 + \frac{1}{4} B_U [(\mathbf{S} \cdot \mathbf{S})^2 + c.c.] \Delta_{4\mathbf{Q}, \mathbf{G}}. \end{aligned} \quad (6)$$

Note the umklapp term $\Delta_{4\mathbf{Q}, \mathbf{G}}$, arising directly from the lattice periodicity [12]. This term is crucial in order to

account for the first order phase transition observed at T_{N1} in CuO where a commensurate collinear state is stabilized.

The free energy, $F = F_{2I} + F_{2A} + F_{4I}$, with $A_Q = a(T - T_Q)$ and $\tilde{A}_0 - D_{y0} = a(T - T_0)$, is then numerically minimized. As in Ref. [15], most coefficients are set using analytical solutions associated with phase boundaries of second order transition. For example, setting $T_Q = 1.18$, $D_{yQ} = 0.02$, $B_1 = 0.103$, and $B_2 = 0.011$, reasonable values for the critical temperatures at zero field ($T_{N3} = 1.2$ and $T_{N2} = 1.12$). We also set $D_{zQ} = 0.01$ as we must have $D_{zQ} < D_{yQ}$, while the direction of the spins in the ac plane ($\alpha_{exp} \sim 70^\circ$) [1] is used to determine the ratio $D_{xzQ}/D_{zQ} = -0.42$. The last coefficients are determined using the temperature of the multicritical point (where T_{N2} and T_{N3} boundaries meet) and the maximum field at $T = 0$ K. From this exercise, we find $B_3 = 0.063$ and $B_4 = 0.013$ while $B_5 = 0.1$ was set arbitrarily. Finally, $B_U = 0.035$ is used to obtain $T_{N1} = 0.77$.

Fig. 5 shows the magnetic phase diagram obtained from minimization of the free energy. For comparison, we also present results obtained without the anisotropic terms D_{zQ} and D_{xzQ} (dotted lines). Depending on the scenario considered, we obtain 5 or 6 magnetic phases illustrated in Fig. 4, described by the order parameters listed in Table I. At zero field, both models (with and without D_z and D_{xz}) predict the same phase sequence, consistent with our experimental observations shown in Fig. 2. At low temperatures, a collinear phase AF1 with the moments along \mathbf{b} is predicted (see Fig. 4) while the AF2 phase corresponds to a spiral configuration in agreement with neutron scattering data [6]. According to our numerical calculation, the new intermediate phase AF3

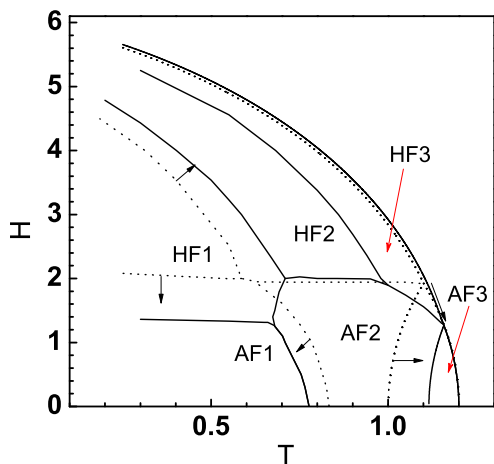


FIG. 5. Magnetic field - temperature phase diagram of CuO for $\mathbf{H} \parallel \mathbf{b}$ derived from the Landau free energy. Dotted lines represent prediction with only one anisotropic term included, D_{yQ} . The solid line is for the case where all anisotropic terms considered.

TABLE I. Order parameters.

state	β	θ	γ	α
AF1	$\pi/4$	$\pi/2$	0	-
AF2	β	0	0	70°
AF3	-	-	0	-
HF1	$\pi/4$	$\pi/2$	$\pi/2$	160°
HF2	β	0	$\pi/2$	70°
HF3	$\pi/2$	0	-	70°

is associated with a collinear phase where only half of the moments order with $\mathbf{S} \parallel \mathbf{b}$. As the field is applied, two spin-flop transitions (AF1 \rightarrow HF1 and AF2 \rightarrow HF2) are found. The comparison of both phase diagrams indicates that the role of the anisotropic terms D_{zQ} and D_{xzQ} is to reduce the critical field of the AF1 \rightarrow HF1 transition, decrease the stability range of the intermediate phase AF3, and lead to a new magnetic order HF3 in which half the moments align into the ac plane. These findings could account for the fact that no spin-flop phase transition has been observed experimentally up to 16 T for the spiral phase AF2.

Our principal conclusions are that a new collinear phase (AF3) has been detected by high resolution ultrasonic velocity measurements which occurs between the paramagnetic and the previously identified spiral phase. The magnetic-field vs temperature phase diagram for $\mathbf{B} \parallel \mathbf{b}$ has also been determined, revealing the existence of a new spin-flop phase (HF1). Complementary dielectric measurements also confirm that magnetoelectric effects only exist in the non-collinear phase. Verification that the new AF3 phase must exist is achieved by a Landau-type model based on rigorous symmetry arguments. Furthermore, the occurrence of such a collinear state, just above a non-collinear state, is confirmed in well studied frustrated RMnO₃ and RMn₂O₅ systems [20–22], and the kagomé compound Ni₃V₂O₈ [23]. Finally, the proposed model accounts for the experimental phase diagram of CuO determined in this work and is potentially useful for the description of other monoclinic multiferroic systems, in particular MnWO₄ [24] and AMSi₂O₆ [25].

ACKNOWLEDGMENTS

This work was supported by the Natural Science and Engineering Research Council of Canada (NSERC).

* Email address: renan.villarreal@mun.ca

- [1] M. Ain, A. Menelle, B. M. Wanklyn, and E. F. Bertaut, J. Phys.: Cond. Matter **4**, 5327 (1992).
- [2] M. Fiebig, J. Phys. D: Appl. Phys. **38**, R123 (2005).

- [3] T. Kimura, Y. Sekio, H. Nakamura, T. Siegrist, and A. P. Ramirez, *Nat. Mater.* **7**, 291 (2008).
- [4] T. Kimura, T. Goto, H. Shintani, K. Ishizaka, T. Arima, and Y. Tokura, *Nature* **426**, 55 (2003).
- [5] K. Wang, J.-M. Liu, and Z. Ren, *Adv. Phys.* **58**, 321 (2009).
- [6] J. B. Forsyth, P. J. Brown, and B. M. Wanklyn, *J. of Phys. C: Sol. State Phys.* **21**, 2917 (1988).
- [7] P. Babkevich, A. Poole, R. D. Johnson, B. Roessli, D. Prabhakaran, and A. T. Boothroyd, *Phys. Rev. B* **85**, 134428 (2012).
- [8] P. Tolédano, N. Leo, D. D. Khalyavin, L. C. Chapon, T. Hoffmann, D. Meier, and M. Fiebig, *Phys. Rev. Lett.* **106**, 257601 (2011).
- [9] G. Giovannetti, S. Kumar, A. Stroppa, J. van den Brink, S. Picozzi, and J. Lorenzana, *Phys. Rev. Lett.* **106**, 026401 (2011).
- [10] G. Jin, K. Cao, G.-C. Guo, and L. He, *Phys. Rev. Lett.* **108**, 187205 (2012).
- [11] G. Quirion, M. L. Plumer, O. A. Petrenko, G. Balakrishnan, and C. Proust, *Phys. Rev. B* **80**, 064420 (2009).
- [12] M. L. Plumer, *Phys. Rev. B* **78**, 094402 (2008).
- [13] S. G. Condran and M. L. Plumer, *J. Phys.: Cond. Matter* **22**, 162201 (2010).
- [14] G. Quirion, X. Han, and M. L. Plumer, *Phys. Rev. B* **84**, 014408 (2011).
- [15] M. L. Plumer, K. Hood, and A. Caillé, *Phys. Rev. Lett.* **60**, 45 (1988).
- [16] G. Quirion, X. Han, M. L. Plumer, and M. Poirier, *Phys. Rev. Lett.* **97**, 077202 (2006).
- [17] O. Kondo, M. Ono, E. Sugiura, K. Sugiyama, and M. Date, *J. Phys. Soc. Japan* **57**, 3293 (1988).
- [18] X. Rocquefelte, M.-H. Whangbo, A. Villesuzanne, S. Jobic, F. Tran, K. Schwarz, and P. Blaha, *J. Phys.: Cond. Matter* **22**, 045502 (2010).
- [19] A.-M. Pradipto, R. Maurice, N. Guihéry, C. de Graaf, and R. Broer, *Phys. Rev. B* **85**, 014409 (2012).
- [20] D. O'Flynn, C. V. Tomy, M. R. Lees, A. Daoud-Aladine, and G. Balakrishnan, *Phys. Rev. B* **83**, 174426 (2011).
- [21] T. Kimura, G. Lawes, T. Goto, Y. Tokura, and A. P. Ramirez, *Phys. Rev. B* **71**, 224425 (2005).
- [22] Y. Noda, H. Kimura, M. Fukunaga, S. Kobayashi, I. Kagomiya, and K. Kohn, *J. Phys.: Cond. Matter* **20**, 434206 (2008).
- [23] G. Lawes, A. B. Harris, T. Kimura, N. Rogado, R. J. Cava, A. Aharony, O. Entin-Wohlman, T. Yildirim, M. Kenzelmann, C. Broholm, et al., *Phys. Rev. Lett.* **95**, 087205 (2005).
- [24] V. Felea, P. Lemmens, S. Yasin, S. Zherlitsyn, K. Y. Choi, C. T. Lin, and C. Payen, *J. Phys.: Cond. Matter* **23**, 216001 (2011).
- [25] S. Jodlauk, P. Becker, J. A. Mydosh, D. I. Khomskii, T. Lorenz, S. V. Streltsov, D. C. Hezel, and L. Bohatý, *J. Phys.: Cond. Matter* **19**, 432201 (2007).